Assessment of the drag porosity approach to model the atmospheric boundary layer over urban canopies

Quentin Bucquet, Isabelle Calmet, Laurent Perret

Assessment of the drag porosity approach to model the atmospheric boundary layer over urban canopies

Q. BUCQUET[a], I. CALMET[a,b], L. PERRET[a,b]

a. Laboratoire de recherche en Hydrodynamique, Énergetique et Environnement Atmosphérique (LHEEA) - UMR6598 CNRS - Ecole Centrale de Nantes - Nantes, France
b. Institut de Recherche en Sciences et Techniques de la Ville, FR CNRS 2488 (IRSTV) - Ecole Centrale de Nantes – Nantes, France

Résumé :

Le travail présenté ici se place dans un contexte d'étude des écoulements atmosphériques se développant au-dessus de canopées urbaines. Plus précisément, cette étude s'intéresse à l'évaluation du modèle de porosité-traînée implémenté dans le solveur atmosphérique au grandes-échelles ARPS (Advanced Regional Prediction System) avec la littérature et les résultats expérimentaux du projet URBANTURB. L'écoulement au-dessus d'une canopée urbaine idéalisée, se composant d'obstacles cubiques arrangés en quinconce avec une densité au sol de 25% modélisés par l'approche de porosité-traînée est étudié à travers des simulations atmosphériques neutres aux grandes échelles (LES) à haut Reynolds. En plus des statistiques en un point, un intérêt particulier à été dédié à l'évaluation des structures turbulentes cohérentes et de leur échelles caractéristiques, en comparaison avec la littérature. Une étude des spectrogrammes, et des spectres 1D et 2D ont révélé la présence de structures classiques caractéristiques d'écoulements turbulents se développant sur paroi lisse ou rugueuse. Un filtrage spectral des échelles les plus énergétiques a fait apparaître une interaction non-linéaire entre les petites et grosses structures. Le but de ce papier est d'étudier les capacités de l'approche porosité-trainée pour la reproduction d'un l'écoulement instationnaire au-dessus d'une canopée urbaine.

Abstract :

This present work details the assessment of the drag-porosity model implemented in ARPS (Advanced Regional Prediction System) atmospheric LES solver with comparison with literature and previous experimental results obtained from the URBANTURB project. The flow inside an idealized urban canopy consisting of a staggered array of cubes with a plan area density of 25% modelled with the drag-porosity approach immersed into a neutral atmospheric boundary layer at high Reynolds is investigated. Besides one-points statistics, particular interest was given to the assessment of turbulent coherent structures and their characteristic scales with literature. An analysis of spectrograms, one- and two-dimensional spectra revealed the presence of typical structures found in smooth- and rough-wall bounded turbulent flows. Further investigation to identify the interaction mechanisms between large and small scales based on wavelength spectral filtering highlighted a non-linear mechanism as observed in literature. The goal of this paper is to assess the capacity of the drag-porosity approach to compute turbulent flows in the roughness sublayer and surface layer.

Mots clefs : Couche limite atmosphérique, Approche de porosité-traînée, Canopée urbaine, Ecoulements turbulents, Simulations aux grandes-échelles

1 Introduction

The numerical modelling of turbulent transport and mixing processes resulting from the interactions between the urban areas and the atmospheric boundary layer is of great importance for air quality assessment and micro-climate predictions. A wide range of scales, from the large coherent structures of the atmospheric boundary layer to the smaller ones generated within the urban canopy, are involved in the unsteady transfers of mass, heat and momentum. Even with the fastly growing computing resources of new supercomputers during the last decades, the simulation of all scales and their dynamic interactions remains an issue when the studied area extends to the entire city. Unsteady approaches such as large-eddy simulations (LES) that solve the flow characteristics around urban elements are generally limited to the size of a single neighbourhood [10, 9]. Thus, a mesoscale model accounting for the heterogeneity and the main morphological characteristics without necessarily simulating all the details of the urban canopy is needed to represent an entire city.

The drag-porosity approach, initially developped for vegetation canopies, models the presence of obstacles and their influence on the turbulent flow by a drag force that depends on averaged morphological characteristics of the canopy. The principal advantage of this approach is to reduce the computation costs. However, the ability of the drag approach to simulate, without any forcing other than that imposed through the drag coefficient and canopy density, the turbulent exchanges between the urban canopy and the overlying layers and the scales characteristic of those layers remains to be demonstrated.

The objective of this paper is to assess the capacity of the drag-porosity model to simulate rough-wall turbulent flows in the roughness sublayer and the log-layer based on comparisons with literature (through experimental [4, 1] and numerical studies [6, 13] over urban canopies) ; in particular, the existence of typical turbulent structures found in smooth- and rough-wall flows will be assessed.

Section 2 is dedicated to the description of the atmospheric numerical solver ARPS used in this study. The results are given in section 3. Finally, conclusions are drawn in section 4

2 Methods

2.1 Model equations

The code ARPS [24, 25] used in this study is a 3D atmospheric Large-Eddy simulation (LES) model developed by the Center for Analysis and Prediction of Storms (CAPS, University of Oklahoma) which can be used for mesoscale simulations at high resolution. The non-hydrostatic compressible filtered Navier-Stokes equations are solved in terrain-following coordinates. Based on the drag force approach introduced in ARPS [7] the momentum equation for a neutral atmosphere (e.g. ignoring buoyancy effects) writes for i^{th} component as :

$$\overline{\rho}\left(\frac{\partial \widetilde{u}_i}{\partial t} + u_j \frac{\partial \widetilde{u}_i}{\partial x_j}\right) = F_{P_i} + F_{C_i} - \frac{\partial \tau_{ij}}{\partial x_j} - F_{D_i} \tag{1}$$

where over tilded variables are filtered or large-scale variables and simple over barred variables indicate the atmospheric base state. The first term on the right hand side is the pressure-gradient force term F_{P_i}.

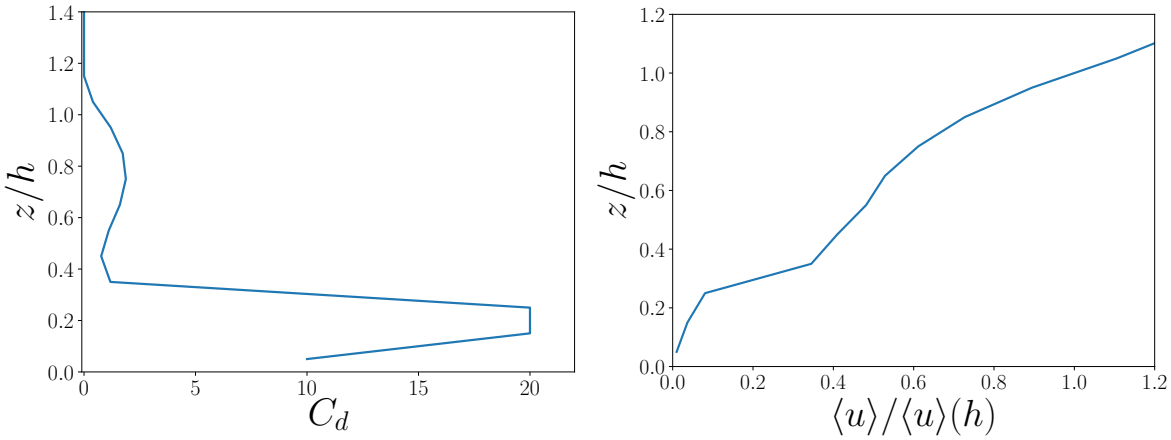

FIGURE 1 – Vertical profiles of C_d for canopy density $\lambda_p = 25\%$ (left); Vertical streamwise velocity profile $\langle u \rangle / \langle u \rangle (h)$ (right).

The Coriolis force term F_{C_i} in equation (1) is expressed as :

$$F_{C_i} = -2\overline{\rho}\epsilon_{ijk}\omega_j(\widetilde{u}_k - \overline{u}_k) \tag{2}$$

where $\vec{\omega}$ is the angular velocity of the earth and ϵ_{ijk} is the alternating unit tensor.

The drag force component F_{D_i} introduced in equation (1) as a sink term for momentum is expressed for urban canopies as :

$$F_{D_i} = 0.5\overline{\rho}C_d(z)a_f(z)\widetilde{u}_i\sqrt{\widetilde{u}_j\widetilde{u}_j} \tag{3}$$

where C_d is the drag coefficient and a_f is the frontal density per unit volume (in m^{-1}), defined as the ratio of the total windward area of the obstacles to the volume of fluid in a cell.

The drag force approach, implemented in ARPS for forest canopies, was adapted to urban-like canopies by [16] so as the mean velocity profiles obtained by ARPS agree with profiles from literature for staggered cube arrays. Various profiles of $C_d(z)$ have been proposed as a function of the packing density λ_p (defined as the plan area occupied by the osbtacles relative to the total surface area). In the present study, the $C_d(z)$ profile for a density of 25% is used (see figure 1).

The SGS stress τ_{ij} in equation (1) is modelled by :

$$\tau_{ij} = -\overline{\rho}\nu_t\left(\frac{\partial\widetilde{u}_i}{\partial x_j} + \frac{\partial\widetilde{u}_j}{\partial x_i}\right) \tag{4}$$

where the SGS eddy viscosity ν_t is modelled with a velocity scale based on the SGS turbulent kinetic energy e :

$$\nu_t = 0.1 l_m\sqrt{e} \tag{5}$$

with the SGS mixing length l_m that depends on grid size.

The SGS turbulent kinetic energy budget equation is expressed as :

$$\frac{\partial e}{\partial t} + \widetilde{u}_j \frac{\partial e}{\partial x_j} = -\tau_{ij} \frac{\partial \widetilde{u}_i}{\partial x_j} + \frac{\partial}{\partial x_j}\left(2\nu_t \frac{\partial e}{\partial x_j}\right) - C_\epsilon \frac{e^{\frac{3}{2}}}{l_\epsilon} - C_d(z) a_f(z) e \sqrt{\widetilde{u_j}\widetilde{u_j}} \tag{6}$$

The terms on the right hand side correspond respectively to the shear stress production, the turbulent transport, the dissipation rate and the SGS energy cascade. This later, based on the sectional drag coefficient, depends on the form drag produced by the canopy elements.

2.2 Numerical details

The present simulations are performed over flat terrain modelling homogeneous urban canopies under neutral atmospheric conditions. The packing density is chosen to be of 25% within $280h \times 140h \times 140h$ m^3 = $2.8\delta \times 1.4\delta \times 1.4\delta$ m^3 domains (h being the canopy height and δ the atmospheric boundary layer ABL height given in table 1), with $560 \times 280 \times 59$ grid points in the x (streamwise), y (spanwise) and z (vertical) directions respectively. The horizontal resolution is $\Delta_x = \Delta_y = 5$ m, with a vertical resolution of 1 m below $z = 25$ m and vertical stretching as a function of a hyperbolic tangent above. Here, the packing density is set equal to the frontal area density λ_f (defined as the ratio of the total windward area of the obstacles to the total surface area) as in experimental studies over staggered arrangement of cubes.

The lateral boundary conditions are periodic, bottom and top boundary conditions are rigid walls and a 400 m deep Rayleigh damping layer is set at the upper boundary in order to absorb upward propagating wave and suppress wave reflection from the rigid top boundary. The velocity fields, potential temperature and specific humidity vertical profiles were initialized using a meteorological pre-processor with a constant vertical profile of potential temperature of 300 K, a dry atmosphere and geostrophic wind components of 12 m.s^{-1} in the x-direction, and 0 m.s^{-1} in the y-direction. It is important to note that no Coriolis force is applied in our simulations as this paper aims to compare results obtained from a drag-porosity atmospheric LES model with experimental results obtained from wind tunnel experiments where Coriolis force does not apply and no veering effect of the mean wind profile is observed. Moreover, this work mainly looks at the flow physics in the lower atmospheric boundary layer, a region that does not exceed $z = 300$ m in height, where the veering wind effect remains negligible.

The computation time step was set to $\Delta_t = 0.05\ s$. Simulation was run for 2.7h of dimensional time, which is $200\,000$ steps for the LES. Simulation required approximately 5160 core hours of computational time with a horizontal spatial resolution of $\Delta_x = 5\ m$.

Since the lowest portion of the ABL is considered in this study, namely the RSL and the logarithmic region or inertial layer, we use the canopy-based turnover time $\tau_r = h/u_*$, to assess the statistically steady-state of the dynamic flow field, where h is the canopy height, u_* the friction velocity. In our case, τ_r is 28.9s : hence, the simulation was run for approx $300\tau_r$. Moreover, this simulation was initialized with extrapolated converged fields from coarser horizontal resolutions ($\Delta_x = 10\ m$), run for 5.3 h ($630\tau_r$). By using this grid extrapolation initialization option, we ensure that flow fields quickly reach a statistically quasi-steady state : a time convergence study was performed, but is not presented here. In order to ensure statistical convergence, we choose to average flow quantities over an averaging period of 4000 s (approx. $130\tau_r$).

λ_p	u_*	τ_r	δ	h	δ^+	h^+	z_0/h	d/h
-	m/s	s	m	m	-	-	-	-
25%	0.346	28.9	1000	10	2.20×10^7	2.20×10^5	0.119	0.695

TABLE 1 – Characteristics of the boundary layer.

3 Results

In this section, numerical results obtained with the drag-porosity model are analysed and compared with experimental results to determine if the numerical model used to represent the urban canopy yields comparable results for boundary layer characteristics, local statistics and turbulent structures in the RSL and surface layer. For the sake of clarity, the overtilde on $\widetilde{u_i}$ will be omitted in this section. The streamwise, spanwise and vertical velocity components will be refered as u, v and w respectively. Each flow parameter is decomposed in a mean and a fluctuating part as for the streamwise velocity :

$$u = \langle u \rangle_{x,y,t} + u' \tag{7}$$

Where u is the instantaneous velocity, $\langle u \rangle_{x,y,t}$ the space-time averaged mean and u' the fluctuations. For the sake of clarity, the subscript denoting the averaged quantity will be omitted, as most of the quantities are averaged horizontally and temporally, excepted in few cases when specified.

3.1 Boundary layer characteristics

The main characteristics of the boundary layer studied here are gathered in table 1.

Displacement thickness d and roughness length z_0 have to be determined from the well- known logarithmic law :

$$\langle u \rangle = \frac{u_*}{\kappa} \ln\left(\frac{z-d}{z_0}\right) \tag{8}$$

with the von Kármán constant κ set to 0.4 and the friction velocity, u_* , is estimated from the vertical profile of the Reynolds shear stress in the constant shear stress region, given by :

$$u_* = \frac{1}{h}\int_h^{2h} \sqrt[4]{\langle u'w' \rangle^2 + \langle v'w' \rangle^2 dz} \tag{9}$$

Hence, the roughness length z_0 and the displacement length d are determined by optimizing a logarithmic fit of the averaged-velocity profiles so as to minimize the root mean square error fitting. The value obtained ($z_0/h = 0.119$) shows good match with literature [1, 14]. The value of the displacement length d, which is typically between $0 < d < h$ (here $d = 0.695h$) shows good agreement with the range reported by [15].
Overall, the aerodynamic parameters computed in this study are found to be a well match with results from [11].

The log-law assumes horizontal homogeneity of the flow at a given wall distance z, and is only valid outside the roughness sublayer (RSL). Thus, as per figure 2, the RSL extend up to $(z-d)/z_0 = 10$ ($z/h = 1.88$). This is a typical estimate of the roughness sublayer, as [12] reported a similar extend of

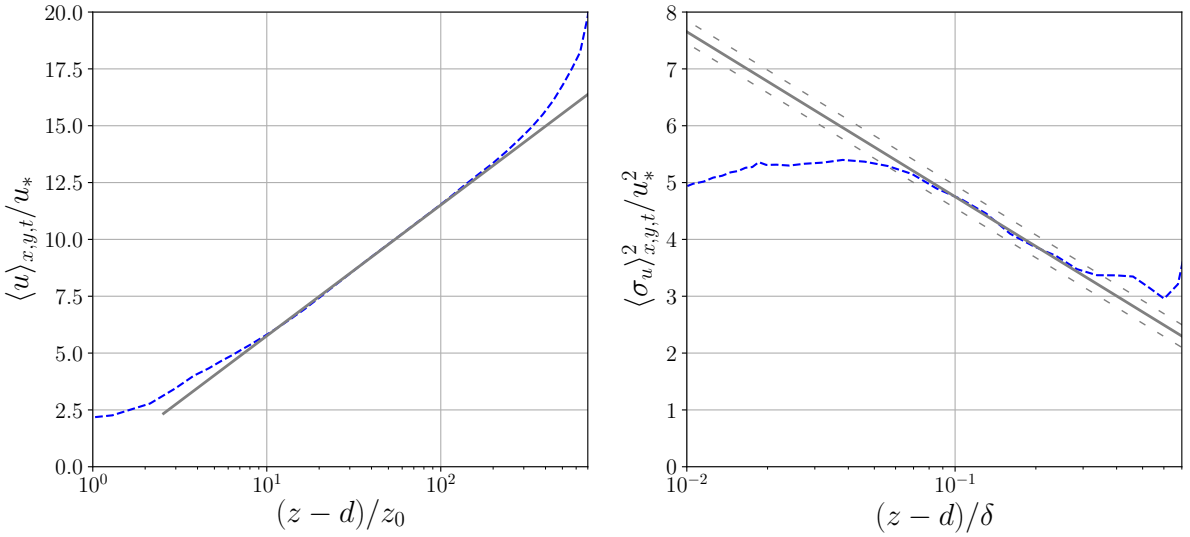

FIGURE 2 – Wall-normal profiles of mean streamwise velocity component (left) and variance of the streamwise velocity component (right). The solid black line in left figure depicts the logarithmic law for the streamwise velocity (equation 8). The solid black line in right figure depicts the logarithmic law for variance with a slope A_1 = 1.26 (equation 10). Dashed black lines depicts a range of $\langle \sigma_u \rangle^2/u_*^2 \pm 0.2$.

the RSL up until $2h - 2.5h$ with Direct Numerical Simulations of cube-roughened walls. Additionally, the log-law is valid up to $(z-d)/z_0 \approx 200$, which is $z/h = 24.5$.

The present boundary layer allows for the existence of an unambiguous log-layer, shown in figure 2, where the wall-normal profile of the averaged streamwise velocity component exhibits a log-law similarity over more than an order of magnitude. A particularly good concordance with experimental results from [1] of the wall-normal velocity profile, RSL and log-layer depths, as well as ABL characteristic parameters is obtained.

Townsend [22] results showed that the presence of self-similar wall-attached eddies (structures scalable with their distance from the wall and, in particular, structures of which streamwise and spanwise scales evolve in the same manner as a function of the wall distance) in the inertial layer leads to a logarithmic wall-normal evolution of both the variance and the mean of the streamwise velocity component. Following these results, a logarithmic law for the variance was proposed by [17], namely :

$$\frac{\langle \sigma_u \rangle^2}{u_*^2} = B_1 - A_1 \ln\left(\frac{z-d}{\delta}\right) \tag{10}$$

and for which one can note here the very good agreement between the variance profile in figure 2. $A_1 = 1.26$ is the slope constant proposed by [17] and B_1 is a constant that depends on the flow geometry and wake parameter (here $B_1 = 1.85$, which falls within the range of [17] when accounting for the error via the use of a range of validity $\langle \sigma_u \rangle^2/u_*^2 \pm 0.2$). A good agreement between the variance profiles and the logarithmic law can be noted for a region that extend over less than an order of magnitude ($(z-d)/\delta = 7 \times 10^{-2} - 3 \times 10^{-1}$).

An overall good collapse of variance profile with this theoretical formula confirms the well-developed high Reynolds number character of the investigated flows, without any unwanted effect of the canopy on the variance evolution, and suggests that the coherent turbulent structures obtained with the drag-porosity approach can be compared to the commonly accepted view of smooth-wall turbulence. Moreover, this

study confirms that the horizontal planes studied in the rest of this paper, located at $z/h = 1.45$ and 4.45 are located in the RSL and the log-layer.

3.2 Instantaneous flow fields

Snapshots of the fluctuating streamwise velocity u'/u_* in top views of the last iteration ($t = 10\,000s$) are discussed here for a qualitative review.

Figure 3 shows the top views of fluctuating streamwise velocity inside the canopy ($z/h = 0.55$), in the RSL ($z/h = 1.45$) and in the log-layer ($z/h = 4.45$). In the log-layer, velocity fluctuations exhibit streaky large scale motions (LSMs), elongated in the streamwise direction with a slightly spanwise meandering effect, characteristic of turbulent boundary layers over smooth planes. In the RSL, u'/u_* exhibits anisotropic structures, showing streaks of low- and high-speed elongated in the streamwise direction with locations matching well that of the upper LSMs found at $z/h = 4.45$: these can be seen as the footprints of the upper LSMs. However it should also be noticed that, in the RSL, smaller and weaker structures (of size of the order of h) co-exist and superimposed itself with larger scales (of size of the order of δ). This superposition, and the fact that sweeping and ejecting motions highlighted by negative fluctuations of wall-normal shear stress $u'w'$ (black contour lines in figure 3d are mostly generated by LSMs is in good agreement with results obtained experimental studies over cube canopies [1]. It appears from figure 3d that sweeps, depicted by intense positive levels of streamwise fluctuating velocity, are produced in the RSL as compact strong packets, while ejections, corresponding to intense negative levels of streamwise fluctuating velocity are much more rare and weaker.

Even if this work does not aim to characterize the turbulent structures and interactions inside the canopy, interesting results can be highlighted from plots in figure 3a at $z/h = 0.55$. An interesting result from this top views concerns the elongated streak sizes broken down with the presence of canopy, and is to be link with [23] who compared results from a smooth model, a roughness model (equivalent to the drag-porosity model presented here) and a cube resolved model. By observing a break down of streaks inside the canopy for both roughness and cube resolved models compared to the smooth model, they conclude that streaks breaking down is not a result of physical obstruction of cubes, but of drag alone. A similar result is obtained here with our canopy configuration.

3.3 Spectral content

The qualitative conclusions based on the instantaneous velocity fields in section 3.2 are now further investigated through a spectral analysis aiming to identify the structuring length scales of the flow, from the small-scale roughness-induced dynamics to the LSMs and VLSMs developing in the boundary layer. In the following, one-dimensional spectra are identified with a subscript, i.e. S_x for a auto-spectra in the x-direction, whereas their two-dimensional counterparts are referred to as S. All spectra presented in figures 4 and 5 are pre-muliplied by wavenumbers $k_{x,y} = 2\pi/\lambda_{x,y}$.

Figure 4 shows the pre-multiplied one dimensional spectra of u as a function of wall-normal distance z/δ and longitudinal and transverse wavenumbers k_x and k_y respectively. Within the canopy, the wavelengths corresponding to the maximum of energy of the longitudinal and transverse spectra of u are both approximately constant with height and of similar sizes : $\lambda_x/h = \lambda_y/h \approx 10$. Above the canopy, for the RSL and the lower part of the log-layer (i.e. $1 \times 10^{-2} < z/\delta < 5 \times 10^{-2}$), the spectrograms of u depict a local maximum and a shift of maximum energy with wall-normal distance z/δ towards large

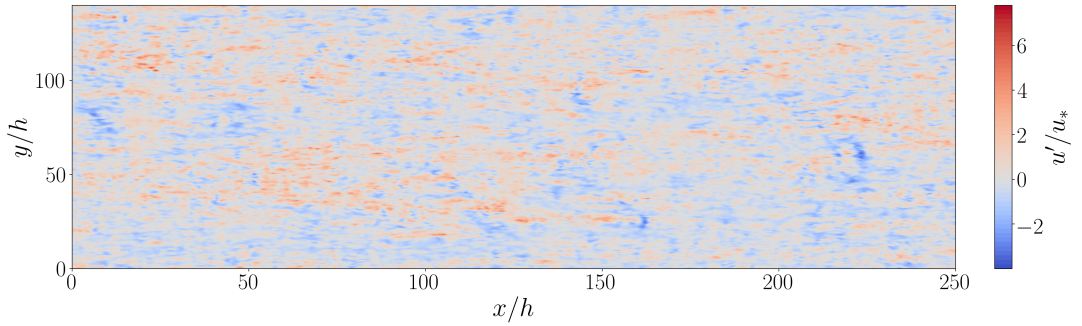

(a) Snapshots of u'/u_* at $z/h = 0.55$

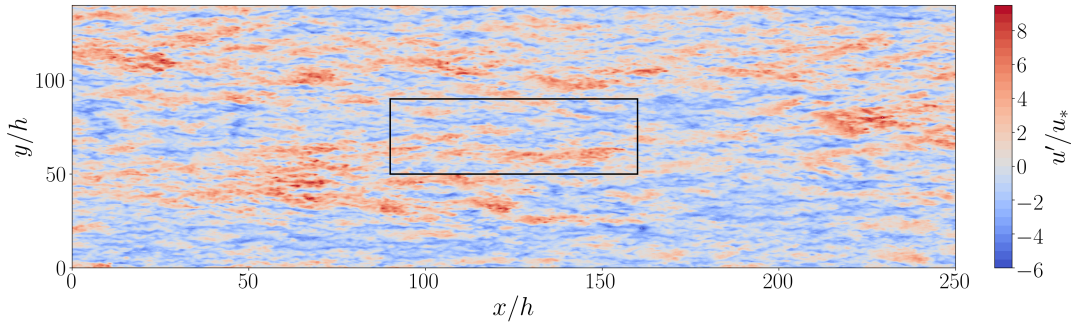

(b) Snapshots of u'/u_* at $z/h = 1.45$

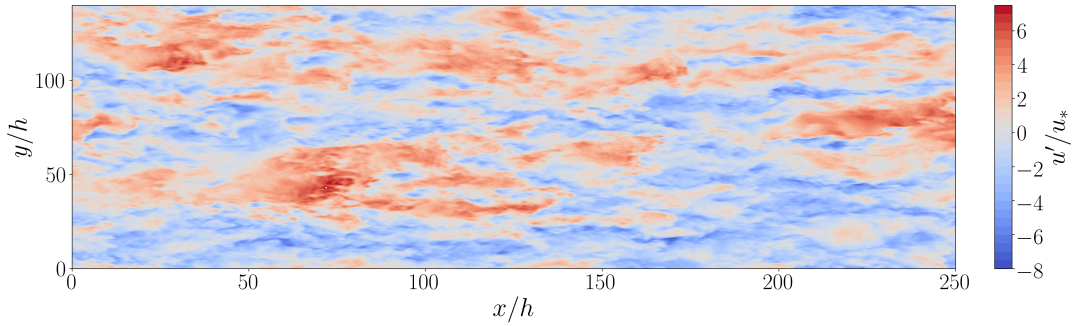

(c) Snapshots of u'/u_* at $z/h = 4.45$

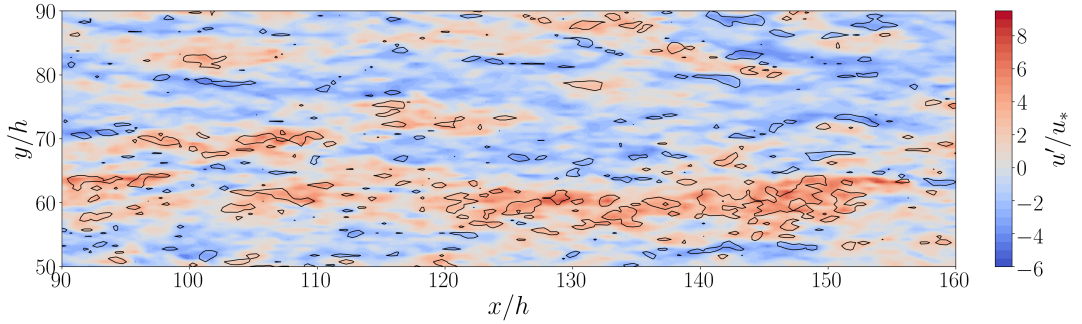

(d) Snapshots of u'/u_* at $z/h = 1.45$ overlaid with isocontours $u'w'$

FIGURE 3 – Instantaneous fluctuations of streamwise velocity normalised by u_* in a $x - y$ plane at : (a) $z/h = 0.55$, (b) $z/h = 1.45$, (c) $z/h = 4.45$. Panel (d) is a close-up view of the centre of the velocity field at $z/h = 1.45$ corresponding to the black squares shown in (b). Solid black contour lines depict intense negative levels of wall-normal shear stress at level $-9.12u_*^2$. Snapshots are taken at $t = 10\,000$s.

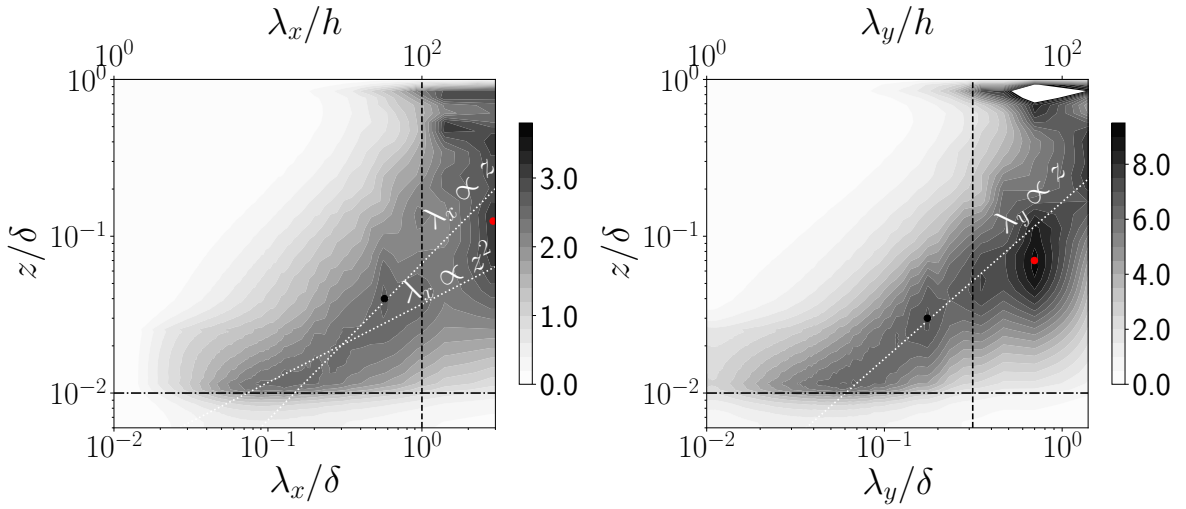

(a) (b)

FIGURE 4 – Normalized pre-multiplied spectrograms of u, $k_{x,y}S_{x,y}(u,u)/u_*^2$, plotted as a function of wall-normal distance z/δ, streamwise wavelength λ_x/δ (a) and transverse wavelength λ_y/δ (b). For clarity, spectra are scaled up by a factor of 10^3. The horizontal dash-dotted line corresponds to the canopy top. Oblique dotted white lines corresponds to $\lambda_x \propto z$ in (a,b) and $\lambda_x \propto z^2$ in (a). Red dot marks the outer peak, black dot marks the inner peak, and the vertical black dashed line shows the location of the spectral filter (λ_c/δ)

.

$0 < z/\delta < 1 \times 10^{-2}$		$1 \times 10^{-2} < z/\delta < 5 \times 10^{-2}$		$5 \times 10^{-2} < z/\delta$	
λ_x/h	λ_y/h	λ_x/δ	λ_y/δ	λ_x/δ	λ_y/δ
≈ 10	< 10	$\propto z^2$	$\propto z$	2.8	7×10^{-1}

TABLE 2 – Streamwise and spanwise wavelengths λ_x and λ_y corresponding to the most energetic scales of u in the different regions of the flow, normalized by the canopy height h or the ABL depth δ

scales. The local maximum wavelength, of the order of a few h, is in agreement with the presence of canopy scales. The wavelengths corresponding to the near-canopy structures increase with the wall distance either as $\lambda_x \propto z^2$ for the streamwise direction or $\lambda_x \propto z$ in the transverse direction (oblique dotted line in figure 4). This result is in good agreement with the Townsend hypothesis of self-similar structures, which states that self-similar eddies scale with wall-normal distance, and that a linear evolution of peak energy production with z/δ should be observed. Well above the canopy, at $z/\delta > 5 \times 10^{-2}$, most energetic structure' scales are constant with height. Table 2 summarizes the streamwise and spanwise wavelengths corresponding to the most energetic scales and their tendency with height.

The spectrograms of the streamwise velocity also exhibit the presence of both inner and outer peaks, similar to what has been found in high Reynolds number turbulent boundary layers [18]. However, in wind-tunnel studies over staggered cubes (1), this feature has to be taken carefully since spectra do not exhibit the presence of both inner and outer peaks as clearly as in [18]. Inner peaks of streamwise spectra occur at $\lambda_x/\delta = 6 \times 10^{-1}$, at levels of $z/\delta \approx 5 \times 10^{-2}$. The presence of outer peaks can be interpreted as the signature of the VLSMs in the streamwise velocity field whose extent scales with δ, often reported in the literature. Outer peak occurs typically at $z/\delta \approx 1 \times 10^{-1}$. However, the wavelengths correspon-

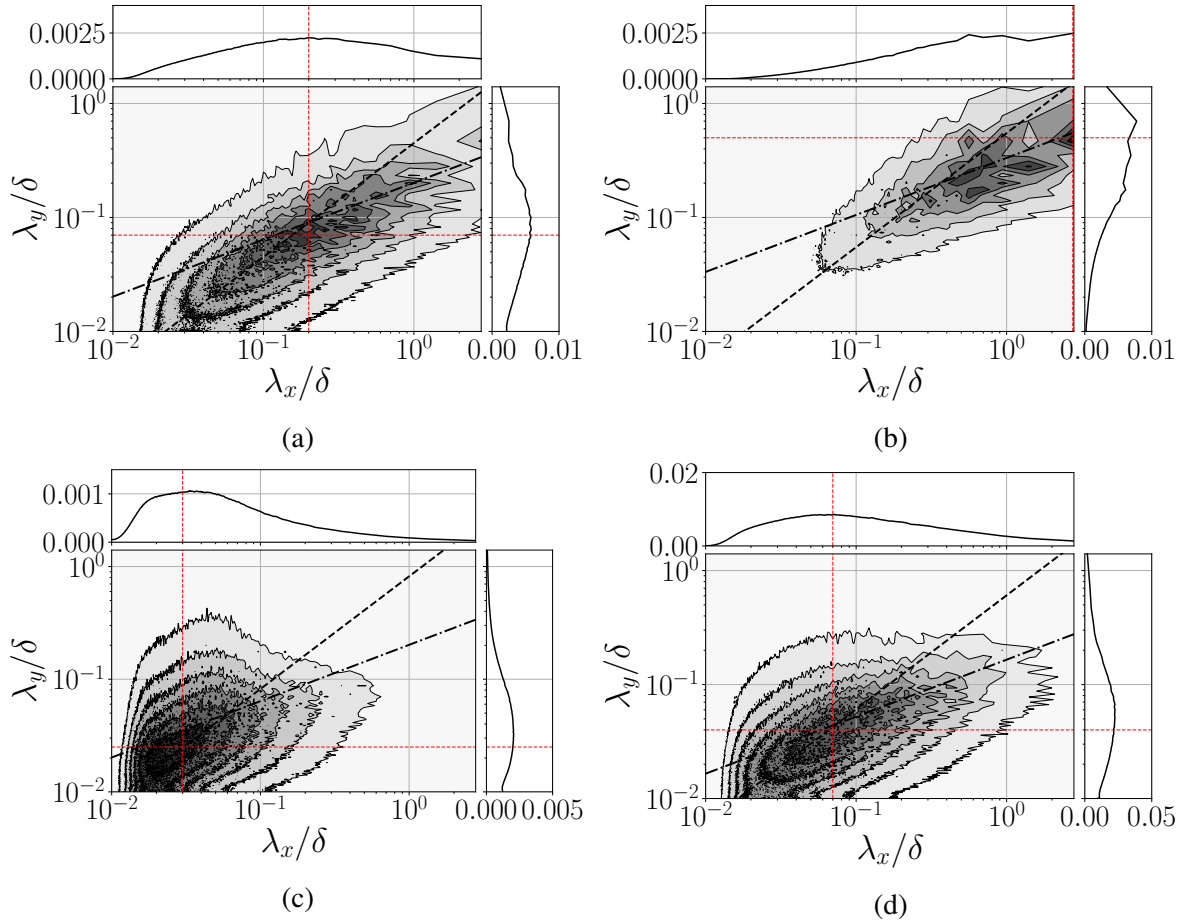

FIGURE 5 – Pre-multiplied auto-spectra in a streamwise-spanwise plane are shown together with one-dimensional pre-multiplied spectra. From top to bottom, (a, b) $k_x k_y S(u, u)$ at $z/h = 1.45$ and $z/h = 4.45$ respectively ; (c) $k_x k_y S(w, w)$ at $z/h = 1.45$; (d) $-k_x k_y S(u, w)$ at $z/h = 1.45$. Oblique dotted white lines corresponds to $\lambda_x \propto \lambda_y$ and $\lambda_x \propto \lambda_y^2$. Red lines intersect at the maximum of the two-dimensional spectra. Contours are shown from 12.5% to 87.5% of the maximum with steps of 12.5%.

ding to the longitudinal VLSMs may be underestimated by this study, since values of $\lambda_x/\delta = 2.8$ are observed, whereas other studies of neutrally stratified, Coriolis-free ABL turbulence, [8] depicted VLSMs streamwise extents that can scale up to $\approx 20\delta$. The influence of the choice of domain dimensions too small for the computation of the largest eddies is seen here. Indeed, the physical domain, of about $(L_x; L_y) = (2.8\delta, 1.4\delta)$ is not extended enough to retain the development of VLSMs : this is why outer peaks are capped at $\lambda_x/\delta = 2.8$. For spanwise spectra, the problem of domain size does not seem to affect the location of the outer peak, it scales with size lower than the spanwise extent : $\lambda_y/\delta = 7 \times 10^{-1}$.

In figure $5(a, b)$, pre-multiplied two-dimensional auto-spectra of u are considered, in two streamwise-spanwise planes at $z/h = 1.45$ and $z/h = 4.45$ corresponding to the RSL and the log-layer respectively. The spectral content within the logarithmic layer ($z/h = 4.45$) and its capacity to reproduce coherent turbulent structures observed in the literature is first discussed here, with figure $5(b)$. Auto-spectra of u in the log-layer exhibit the presence of a peak of maximum energy centered around $\lambda_x = 2.8\delta$ and $\lambda_y = 0.5\delta$ relative to the spectral signature of LSMs and VLSMs that shows good coherence with the spectrograms of figure 4. Analysis of the two-dimensional auto-spectra of u yields the existence of an increasing anisotropy of the structures associated with scales up to $\lambda_x/\delta = 2.8$, since the ridge of

maximum energy follows a $\lambda_x \propto \lambda_y^2$ scaling law. The result of this trend is an increasing elongation of low- and high-momentum regions as they get wider. However, at larger scales, in their study of high Reynolds number boundary layers over smooth walls, [5] predict that energy crest should depart from the $\lambda_x \propto \lambda_y^2$ scaling law to a self-similar law. Due to the limited streamwise extent of the computational domain, such a trend can not be confirmed here.

Figure $5(a)$ of the pre-multiplied auto-spectra of u within the RSL ($z/h = 1.45$), show some important differences with characteristics of LSMs and VLSMs developing in the log-layer. The same comment about the anisotropy of large-scale structures ($\lambda_x > 0.2\delta$), scaling with $\lambda_x \propto \lambda_y^2$ is still valid in the RSL. For smaller structures however, it seems that the ridge of maximum energy is following self-similar trend, hence leading to the coexistence of both non self-similar and self-similar eddies. This coexistence was first observed by [5] in 2D-spectra of experimental and DNS results of low- and high-Reynolds number turbulent wall-bounded flows. Another interesting feature is the shift in energy peak with towards smaller wavelengths ($\lambda_x = 20h$, $\lambda_y = 7h$) compared to the log-layer : the presence of obstacles reduces the impact of LSMs footprints in the RSL and enhances the contribution of canopy-induced turbulent structures. This observation is coherent with the "two-scale" behavior brought forward by [21] that suggest that the large-scale structures existing in the logarithmic layer leave a strong imprint on the flow in the RSL and coexist with structures of similar characteristics and energy yet at smaller scales.

To investigate wall-normal interactions between canopy and RSL, organized mainly in low-velocity upward ejections and high-velocity downward sweeps, auto-spectra of the wall-normal component and co-spectra of u and w are plotted in a streamwise-spanwise plane $z/h = 1.45$ in figure $5(c, d)$.

Auto-spectra of wall-normal component are characterized by a range of energetic scales of about 0.01δ - 0.06δ, e.g. of the order of few h, for both streamwise and spanwise components. More precisely, maximal energy of w is obtained for (λ_x, λ_y) = $(0.03\delta, 0.025\delta)$ = $(3h, 2.5h)$. This highlights that scales related to wall-normal transport of momentum, and by extension to ejections and sweeps, are associated with canopy interactions. Additionally, a trend following closely the scaling law $\lambda_x \propto \lambda_y$ that puts in evidence the existence of a self-similarity in the wall-normal component is observed here, and a near isotropic behavior is also depicted in figure $5(d)$.

Concerning the pre-multiplied co-spectra $-k_x k_y S(u, w)/u_*^2$ in the RSL plotted in figure $5(c)$, red lines depict the presence of a maximum peak, scaling with $\lambda_x = 0.07\delta = 7h$ and $\lambda_y = 0.04\delta = 4h$, of the order of few h. The energetic structures related to cross-correlation between u and w are scaled in between crest scales of w ($\approx 3h$) and crest scales of u ($\approx 10h$). The double effect of u and w in the co-spectra is also brought forward with a trend following a $\lambda_x \propto \lambda_y$ scaling law for smaller structures (as for auto-spectra of u and w) but that departs into a $\lambda_x \propto \lambda_y^2$ scaling law for larger structures (as for auto-spectra of u). Finally, a comment can be made on sweeps and ejections' sizes inside the RSL : since it is found in figure $5(a)$ that the most energetic eddies depict the presence of footprints of LSMs inside the RSL of about $10h - 15h$ depending on canopy density, it becomes clear that the presence of wall-normal exchanges such as sweeps and ejections is closely related to the generation of LSMs, or at least their imprint inside the RSL. This shows good agreement with observations made for instantaneous velocity fields in section 3.2.

3.4 Interaction between the most energetic scales

Recent studies of high-Reynolds wall-bounded flows have evidenced the existence of an interaction mechanism that resembles an amplitude modulation process of the most energetic near-wall scales by the most energetic scales present in the outer region (see 18, 2, 3 among others). The capacity of the drag-porosity model to reproduce this key feature, which suggest that the near-wall turbulence is triggered by the largest scales of the flow through a phase relationships, is presented here.

The spectral analysis presented in the previous sections clearly showed the distinct signature of both the near-canopy turbulence and that related to ABL-scales through the presence of two clear peaks in the spectra. Therefore, following [18], the scale separation is performed here via the use of low-pass filter to extract from the velocity field the large-scale component u'_L associated with the largest energetic scales and decompose, for instance, the instantaneous streamwise velocity u into a space-time averaged mean $\langle u \rangle_{x,y,t}$, large-scale fluctuations u'_L and small-scale fluctuations u'_S :

$$u = \langle u \rangle_{x,y,t} + u'_L + u'_S \tag{11}$$

The cut-off wavelength of the low-pass filter is determined using the pre-multiplied spectrograms of streamwise velocity presented above in figure 4, and is chosen so as to separate the most energetic scales present above the logarithmic layer (outer peaks highlighted in red in the figure) and those in the near-canopy region (inner peaks in black). The dotted black lines in figure 4 show the location of the cut-off, chosen to be $\lambda_c = \delta$. [18] originally proposed to use the correlation coefficient between the large scale component u'_L and the low-pass filtered envelope of the small scales u'_S, the so-called amplitude modulation coefficient, as an indicator of the existence and the importance of the amplitude modulation mechanism. They later showed that the cross-correlation $\langle u'_L u'^2_S \rangle$, resulting from the scale-decomposition of the third-order moment $\langle u'^3 \rangle = \langle u'^3_L \rangle + 3\langle u'_L u'^2_S \rangle + \langle u'^2_L u'_S \rangle + \langle u'^3_S \rangle$ was directly related to the degree of amplitude modulation [19]. This latter approach is employed here to quantify amplitude modulation of the (small) near-canopy scales by the (large) ABL scales. The investigation is extended to the three velocity components using the same filtering method.

Figure $6(a)$ shows the scale-decomposed skewness factor of the streamwise velocity. It appears that the decomposed skewness exhibits a peak at the canopy top ($z/h = 1$) that is most largely due to the combined contribution of the small-scale component $\langle u'^3_S \rangle$ and the cross-term $\langle u'_L u'^2_S \rangle$. The combination of this strongly positive u'_S skewness and strongly negative w' skewness (not shown here) indicates that the predominance of intermittent downward moving gusts (sweeps) is mainly influenced by small-scales. Both quantities become negative above, at $z/h \approx 2$ for $\langle u'^3_S \rangle$ and above $6h$ for the cross-term, thus showing similarities with the skewness profile of a mixing layer, which agrees with [20] and [3]. Alternatively, the large-scale component and the cross-term $\langle u'^2_L u'_S \rangle$ contribute a negligible amount to the skewness in the RSL, and a non-negligible contribution of $\langle u'^3_L \rangle$ is observed only in the log-layer. The cross-term $\langle u'_L u'^2_S \rangle$ represent the non-linear effect of large-scale motions onto smaller scales : its non-negligible wall-normal profile could suggest a top-down mechanism such as amplitude modulation, as it was suggested by [19].

The non-linear term in the skewness decomposition responsible for the interaction between large- and small-scales and its influence on all three velocity components is further investigated in figure $6(b)$.

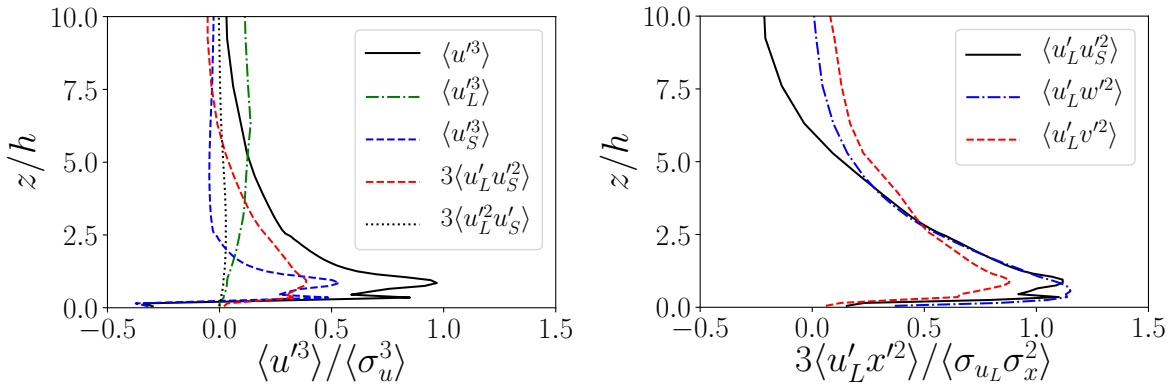

(a) (b)

FIGURE 6 – (a) : skewness decomposition of the streamwise velocity $\langle u'^3 \rangle$ in small-scale skewness $\langle u'^3_S \rangle$, large-scale skewness $\langle u'^3_L \rangle$, and cross-terms $3\langle u'_L u'^2_S \rangle$ and $3\langle u'^2_L u'_S \rangle$. (b) : non-linear cross-terms of the skewness decomposition, $\langle u'_L u'^2_S \rangle$ (black line), $\langle u'_L v'^2 \rangle$ (red dashed line) and $\langle u'_L w'^2 \rangle$ (blue dashed-dotted line). All components are spatially and temporally averaged, and normalized by $\langle \sigma_u^3 \rangle$ (a), or $\langle \sigma_{u_L} \sigma_x^2 \rangle$ (b).

In particular, the non-linear interaction between the large-scale momentum motions and the spanwise ($\langle u'_L v'^2 \rangle$) and the vertical ($\langle u'_L w'^2 \rangle$) non-filtered velocity component is compared with $\langle u'_L u'^2_S \rangle$. Similarly as in the literature [20, 2], the interaction between large-scales and small-scales in the RSL occurs in a similar manner for all flow components.

4 Conclusion

Simulations of the atmospheric boundary layer developing over urban canopies modelled using a drag-porosity approach with the atmospheric LES solver ARPS served as a basis to assess the capacity of such a rough-wall model of reproducing the key features of the spatio-temporal organization of these high Reynolds number flows.

Overall, this work assesses the good agreement of the model with literature : one-points statistics yield coherent characteristic parameters with literature, the existence of unambiguous roughness sublayer and log-layer commonly observed in smooth- and rough-wall turbulence, and the presence of coherent turbulent structures that populate those layers. In particular, the presence of elongated low- and high-momentum streaky LSMs and VLSMs was observed through snapshots and a spectral analysis found that these structures scale with δ. The anisotropic, self-similar feature of these eddies show good agreement with literature. The influence of the drag-modelled urban canopy on the overlying layer (in the RSL) appears adequate with previous experimental and numerical studies, with the existence of a “two-scale” behavior where long, streaky LSMs superimpose with smaller, canopy-induced structures. The analysis of the interaction between the most energetic scales (LSMs and canopy-induced scales) has also confirmed the existence of a non-linear interaction mechanism resembling an amplitude modulation mechanism of the small scales by the larger scales, as it was proposed by [18].

If this work proves that the drag-porosity model is able to reproduce all the turbulent features expected in rough-wall turbulence, while saving calculation cost, some important flow characteristics cannot be reproduced, especially within the canopy, such as recirculating regions which is why results obtained in this layer were not analysed in detail in this work. Therefore, some further developments are still needed

to improve the capacity of modern numerical solvers to capture more detailed information.

Acknowledgements

This work was granted access to the HPC resources of CINES under the allocation 2020-A0080100132 and 2021-A0100100132 made by GENCI.

Références

[1] J. Basley, L. Perret, and R. Mathis. Structure of high Reynolds number boundary layers over cube canopies. *Journal of Fluid Mechanics*, 870 :460–491, July 2019. Publisher : Cambridge University Press.

[2] K. Blackman and L. Perret. Non-linear interactions in a boundary layer developing over an array of cubes using stochastic estimation. *Physics of Fluids*, 28(9) :095108, Sept. 2016.

[3] K. Blackman, L. Perret, and R. Mathis. Assessment of inner–outer interactions in the urban boundary layer using a predictive model. *Journal of Fluid Mechanics*, 875 :44–70, Sept. 2019. Publisher : Cambridge University Press.

[4] I. P. Castro, H. Cheng, and R. Reynolds. Turbulence Over Urban-type Roughness : Deductions from Wind-tunnel Measurements. *Boundary-Layer Meteorol*, 118(1) :109–131, Jan. 2006.

[5] D. Chandran, R. Baidya, J. P. Monty, and I. Marusic. Two-dimensional energy spectra in high-Reynolds-number turbulent boundary layers. *Journal of Fluid Mechanics*, 826, Sept. 2017. Publisher : Cambridge University Press.

[6] O. Coceal, A. Dobre, T. G. Thomas, and S. E. Belcher. Structure of turbulent flow over regular arrays of cubical roughness. *Journal of Fluid Mechanics*, 589 :375–409, Oct. 2007. Publisher : Cambridge University Press.

[7] S. Dupont and Y. Brunet. Influence of foliar density profile on canopy flow : A large-eddy simulation study. *Agricultural and Forest Meteorology*, 148(6) :976–990, June 2008.

[8] J. Fang and F. Porté-Agel. Large-Eddy Simulation of Very-Large-Scale Motions in the Neutrally Stratified Atmospheric Boundary Layer. *Boundary-Layer Meteorology*, 155, June 2015.

[9] M. G. Giometto, A. Christen, P. E. Egli, M. F. Schmid, R. T. Tooke, N. C. Coops, and M. B. Parlange. Effects of trees on mean wind, turbulence and momentum exchange within and above a real urban environment. *Advances in Water Resources*, 106 :154–168, Aug. 2017.

[10] M. G. Giometto, A. Christen, C. Meneveau, J. Fang, M. Krafczyk, and M. B. Parlange. Spatial Characteristics of Roughness Sublayer Mean Flow and Turbulence Over a Realistic Urban Surface. *Boundary-Layer Meteorol*, 160(3) :425–452, Sept. 2016.

[11] C. S. B. Grimmond and T. R. Oke. Aerodynamic Properties of Urban Areas Derived from Analysis of Surface Form. *Journal of Applied Meteorology and Climatology*, 38(9) :1262–1292, Sept. 1999. Publisher : American Meteorological Society Section : Journal of Applied Meteorology and Climatology.

[12] U. Ismail, T. A. Zaki, and P. A. Durbin. The effect of cube-roughened walls on the response of rough-to-smooth (RTS) turbulent channel flows. *International Journal of Heat and Fluid Flow*, C(72) :174–185, 2018.

[13] M. Kanda. Large-Eddy Simulations on the Effects of Surface Geometry of Building Arrays on Turbulent Organized Structures. *Boundary-Layer Meteorol*, 118(1) :151–168, Jan. 2006.

[14] M. Kanda, R. Moriwaki, and F. Kasamatsu. Large-Eddy Simulation of Turbulent Organized Structures within and above Explicitly Resolved Cube Arrays. *Boundary-Layer Meteorology*, 112(2) :343–368, Aug. 2004.

[15] S. Leonardi and I. P. Castro. Channel flow over large cube roughness : a direct numerical simulation study. *Journal of Fluid Mechanics*, 651 :519–539, May 2010.

[16] M. Maché. *Représentation multi-échelles des transferts entre couche de canopée urbaine et atmosphère à l'échelle de la ville*. PhD thesis, Bretagne Loire, Nantes, 2012.

[17] I. Marusic, J. P. Monty, M. Hultmark, and A. J. Smits. On the logarithmic region in wall turbulence. *Journal of Fluid Mechanics*, 716, Feb. 2013. Publisher : Cambridge University Press.

[18] R. Mathis, N. Hutchins, and I. Marusic. Large-scale amplitude modulation of the small-scale structures in turbulent boundary layers. *Journal of Fluid Mechanics*, 628 :311–337, June 2009. Publisher : Cambridge University Press.

[19] R. Mathis, I. Marusic, N. Hutchins, and K. R. Sreenivasan. The relationship between the velocity skewness and the amplitude modulation of the small scale by the large scale in turbulent boundary layers. *Physics of Fluids*, 23(12) :121702, Dec. 2011. Publisher : American Institute of Physics.

[20] L. Perret and F. Kerhervé. Identification of very large scale structures in the boundary layer over large roughness elements. *Exp Fluids*, 60(6) :97, May 2019.

[21] R. T. Reynolds and I. P. Castro. Measurements in an urban-type boundary layer. *Exp Fluids*, 45(1) :141–156, July 2008.

[22] A. A. Townsend. *The structure of turbulent shear flow*. Cambridge monographs on mechanics and applied mathematics. Cambridge University Press, Cambridge [Eng.] ; New York, 2nd ed edition, 1976. OCLC : 1937010.

[23] J. Varghese and P. A. Durbin. Representing surface roughness in eddy resolving simulation. *J. Fluid Mech.*, 897 :A10, Aug. 2020.

[24] M. Xue, K. K. Droegemeier, and V. Wong. The Advanced Regional Prediction System (ARPS) – A multi-scale nonhydrostatic atmospheric simulation and prediction model. Part I : Model dynamics and verification. *Meteorology and Atmospheric Physics*, 75(3) :161–193, Dec. 2000.

[25] M. Xue, K. K. Droegemeier, V. Wong, A. Shapiro, K. Brewster, F. Carr, D. Weber, Y. Liu, and D. Wang. The Advanced Regional Prediction System (ARPS) – A multi-scale nonhydrostatic atmospheric simulation and prediction tool. Part II : Model physics and applications. *Meteorology and Atmospheric Physics*, 76(3) :143–165, Apr. 2001.